Wireless Power Transfer

REVIEW

Open Access

https://doi.org/10.48130/wpt-0024-0009

Wireless Power Transfer **2024**, 11: e009

Perspectives on control strategies for CC-CV charging in Resonant Inductive Power Transfer systems: a review of SS-RIPT configuration

Avishek Munsi, Sushan Pradhan and Kunwar Aditya*

Transportation Electrification Lab (T.E.L), Department of Electrical Engineering, IIT Jodhpur, Rajasthan, India

* Corresponding author, E-mail: kunwar.aditya@iitj.ac.in

Abstract

This paper explores control strategies for Resonant Inductive Power Transfer (RIPT) systems, focusing on achieving Constant Current Constant Voltage (CC-CV) charging for batteries. Wireless power transfer, particularly via RIPT, is gaining traction for charging Electric Vehicles (EVs), Unmanned Aerial Vehicles (UAVs), and consumer electronics. The study investigates direct and indirect control methods for RIPT systems, concentrating on the series-series RIPT (SS-RIPT) configuration. Through simulations and analysis, the paper showcases the implementation of primary side indirect control for CC-CV charging of Li-Ion batteries, offering insights into its feasibility and effectiveness. The findings contribute to advancing the understanding of control strategies in RIPT systems, facilitating the optimization of charging efficiency and enhancing user experience in wireless charging applications.

Citation: Munsi A, Pradhan S, Aditya K. 2024. Perspectives on control strategies for CC-CV charging in Resonant Inductive Power Transfer systems: a review of SS-RIPT configuration. *Wireless Power Transfer* 11: e009 https://doi.org/10.48130/wpt-0024-0009

Introduction

Wireless power transfer, especially via resonant inductive power transfer (RIPT), is becoming increasingly popular for charging various devices such as Electric Vehicles (EVs), Unmanned Aerial Vehicles (UAVs), and consumer electronics such as cellphones[1,2]. This technology offers users a safe and efficient charging experience. With the charging process automated and free from constant user intervention, wireless charging addresses the range anxiety problem in electric vehicles and extends the flight time of UAVs[3,4]. For consumers, eliminating charging cables means no more hassle and clutter, keeping their charging areas clean and organized. Figure 1 shows the block diagram of a typical RIPT-based wireless charger.

In Fig. 1, power is transferred from the transmitter to the receiver through resonant inductive coupling. It consists of two inductors that are magnetically coupled through the principle of electromagnetic induction. The air gap between the transmitter and receiver inductors is significantly larger than a conventional transformer. To improve the system's efficiency, both inductors are made to resonate with a bank of capacitors in the transmitter and receiver circuits. These capacitors can be connected to the inductors in a series, parallel, or a combination of series-parallel configuration, resulting in multiple resonant topologies.

For charging applications, load on the RIPT system is some kind of energy storage device. Due to their high energy density and power density, Li-ion batteries are a popular choice for energy storage devices in electric vehicles, UAVs, and consumer electronics[5–8]. Li-Ion batteries are charged using a Constant Current Constant Voltage (CC-CV) method which is shown in Fig. 2.

In Fig. 2, V represents the battery's rated voltage, I denotes the battery current and R indicates the equivalent resistance variation during the CC-CV charging operation of a lithium-ion (Li-Ion) battery. The battery is initially charged with a constant current until its terminal voltage reaches the rated voltage. Subsequently, the charger transitions to a constant voltage output, maintaining the terminal voltage until the battery achieves full charge. This charging technique, known as CC-CV (constant current-constant voltage), leads to an exponential rise in the terminal resistance observed by the charger, depicted by the red curve in Fig. 2. Consequently, the RIPT (Resonant Inductive Power Transfer) system must be controlled to operate in CC-CV mode.

This paper presents a review of control methods applicable to RIPT systems for charging batteries using the CC-CV mode. Referring to Fig. 1, RIPT systems can be implemented in various configurations depending on the choice of the power converter and compensation topology, it is impractical to address control strategies for every circuit configuration. Therefore, this paper focuses solely on the control method for the Series-Series RIPT (SS-RIPT) system. For the DC-AC converter, H-Bridge topology and for AC-DC converter a Full-Bridge rectifier will be considered. The main contribution is identifying the control variables and utilizing them to achieve the CC-CV mode of operation.

The control strategies for Resonant Inductive Power Transfer (RIPT) systems present a significant concern, and existing literature has yet to address all control strategies comprehensively in a single paper. There is a need for a thorough discussion of these strategies, including their advantages, limitations, and implementation examples, within a single paper. Addressing this gap is essential for advancing future research in this area, which underscores the importance of this review.

Identifying control variables of the SS-RIPT system

Figure 3 shows the SS-RIPT-based wireless charger[9–11]. In Fig. 3, only the DC to DC stage has been considered, and the front-end converter (EMI + PFC) stage has been neglected. In Fig. 3, the symbols V_P and I_P denote the primary side voltage and current, while V_S and I_S represent the secondary side voltage and current, respectively. L_P and L_S refer to the primary and secondary side inductances, and C_P and C_S indicate the primary and secondary side capacitances.

Since the transmitter and receiver sides are mutually coupled through electromagnetic field, therefore battery voltage (V_{Batt}) and battery current (I_{Batt}) can be controlled directly by sensing the V_{Batt} and I_{Batt} or it can be controlled indirectly by sensing the current and

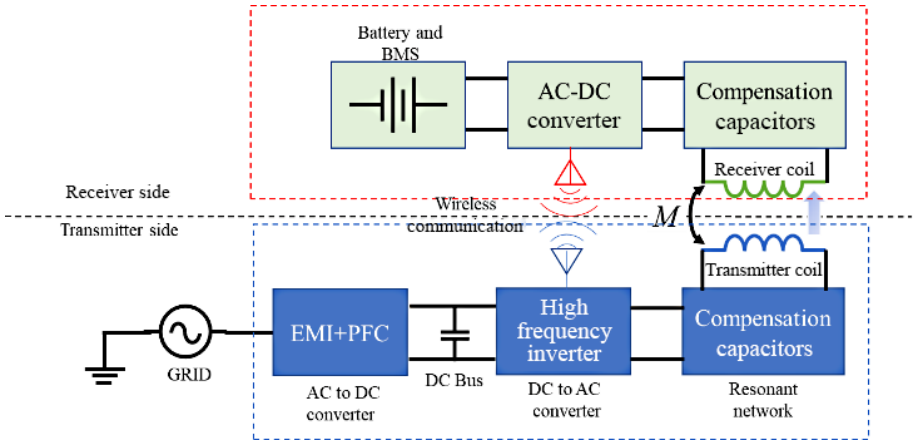

Fig. 1 Block diagram of RIPT based wireless charger.

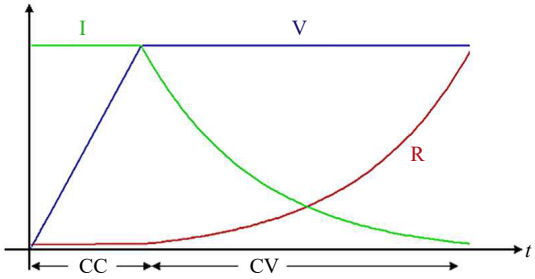

Fig. 2 CC-CV charging operation.

voltage of the resonant tank such as I_P, V_P, I_S, and Vs. Figure 4 shows the electrical equivalent circuit of the SS-RIPT link.

In Fig. 4, R_L is the equivalent resistance of the battery seen by the secondary side, given by Eqn (1).

$$R_L = \frac{8}{\pi^2} R_{Batt} \tag{1}$$

The fundamental components of V_S and I_S are related to V_{Batt} and I_{batt} respectively using Eqns (2) and (3).

$$V_S = 4\frac{V_{Batt}}{\pi} \tag{2}$$

$$I_S = \pi\frac{I_{Batt}}{2} \tag{3}$$

Referring to Fig. 4, at resonance,

$$V_s = |\omega M I_P| \tag{4}$$

$$V_P = |\omega M I_S| \tag{5}$$

By utilizing Eqns (1)–(5), the relationship between battery voltage and current can be established with primary side voltage and current, as demonstrated in Eqns (6) and (7).

$$I_{Batt} = \frac{2}{\pi}\frac{V_P}{\omega M} \tag{6}$$

$$V_{Batt} = \frac{\pi}{4}\omega M I_P \tag{7}$$

Relationships in Eqn (2), (3), (6) and (7) can be utilized to control the battery voltage and current from the resonant tank variables.

It should be noted that battery current/voltage can also be controlled indirectly by sensing DC link voltage V_{DC} and DC link current I_{DC}. However, for this article, the sole focus was on direct control by sensing V_{Batt} and I_{Batt} and indirect control by sensing resonant tank variables. Figure 5 shows the overall block diagram of the CC-CV controller.

In Fig. 5, a voltage/current controller enables the comparison between the measured output voltage/current and the desired values. The outputs of the controller determine the duty cycle for the PWM (Pulse Width Modulation) modulator. This duty cycle is then compared with a ramp signal to generate PWM pulses for the inverter or rectifier, which charges the battery. The PWM block generates a quasi-square wave at the output of the converter as shown in Fig. 6.

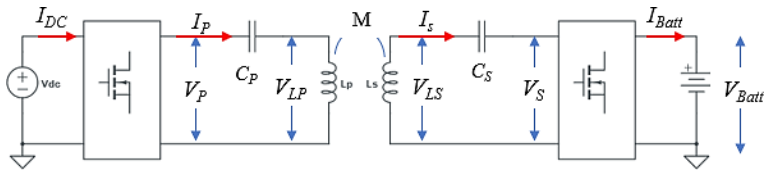

Fig. 3 SS-RIPT based charger.

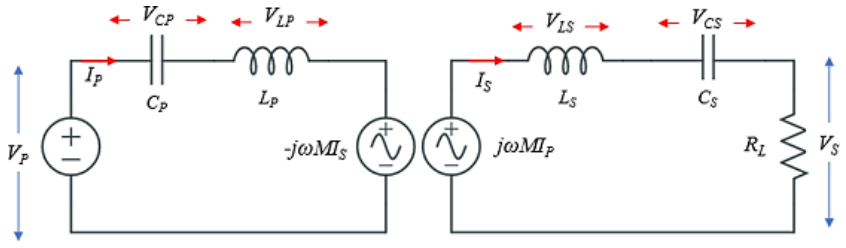

Fig. 4 Simplified equivalent circuit of the SS-RIPT system.

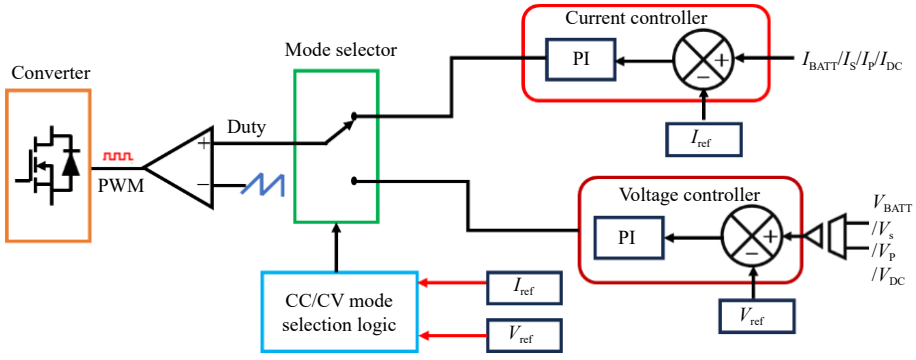

Fig. 5 CC-CV controller.

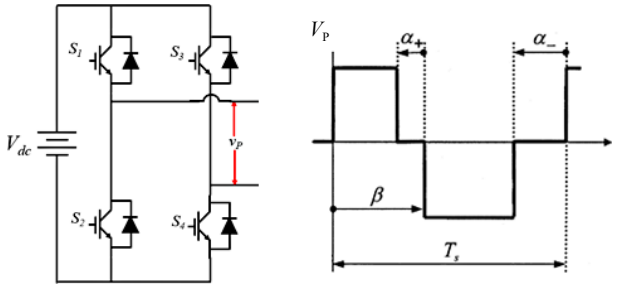

Fig. 6 Quasisquare output voltage waveform of a resonant inverter.

As shown in Fig. 6, output voltage and thus current can be regulated by four control variables α+, α-, and β, and the switching period (T_s). Three types of PWM are possible namely: Symmetric Voltage Cancellation (SVC) also known as Phase shift (PWM), Asymmetrical Voltage Cancellation (AVC), and Asymmetrical Duty Cycle (ADC). Detailed descriptions of these PWM techniques have been previously reported[12,13]. In Fig. 5, a selection logic is incorporated to switch between Constant Current (CC) and Constant Voltage (CV) modes based on the battery's state of charge.

Control strategies in resonant inductive power transfer (RIPT) systems are primarily classified into three types, depending on which side's converter is being controlled: primary side control, secondary side control, and dual side control. Primary side control involves regulating the converter of the transmitter (i.e., the DC-AC converter), while secondary side control focuses on managing the converter of the receiver side (i.e., the AC-DC converter). Dual side control, on the other hand, entails controlling both the transmitter and receiver converters simultaneously.

Based on the choice of control signal (reference signals), Table 1 categorizes the control method for SS-RIPT chargers. In Table 1, direct refers to sensing the battery voltage and current directly for feedback and indirect control refers to sensing signal other than load (battery) voltage and current.

Existing primary side direct control strategies typically rely on wireless communication modules, such as Wi-Fi and ZigBee. In these strategies, charging information is wirelessly transmitted from the secondary side to the primary side and is then used as reference signals for the controller. Although this is a well-established technical solution, many studies have thoroughly analyzed the primary side direct control methods[14–17], and certain challenges persist. These challenges include the additional cost of hardware and software for wireless communication modules, potential communication instability due to strong magnetic field interference, and the unsuitability of wireless communication for specific applications such as underwater or aerospace environments.

To address these issues, some studies have introduced primary side indirect control methods. In Madawala et al.[18], the output power is regulated through the power-frequency droop characteristic of the wireless charging system, eliminating the need for a dedicated communication link. In Chow et al.[19], transmitter-side electrical information is used to regulate the power consumption on the receiver side. However, these methods focus solely on adjusting the output power without addressing the control of charging current and voltage. In Madawala & Thrimawithana[20], a phase-shifted full-bridge inverter is used to achieve constant voltage (CV) charging for the RIPT system, based on the estimated charging voltage from the primary side. However, no further analysis of constant current (CC) charging is provided. In Song et al.[21], while the primary side controller is capable of CC/CV charging for the SS/SP compensated RIPT system, it requires the estimation of load resistance and mutual inductance to control the charging current and voltage. This, in turn, necessitates additional hardware for load resistance estimation and mutual inductance identification, increasing system complexity and overall cost. In Li et al.[22], a primary side indirect control method is proposed to achieve CC/CV charging for the SS compensated RIPT system without the need for load identification, mutual inductance estimation, or dual-side communication.

Table 1. Classification of control method for SS-RIPT systems.

Type of control		Control variables
Direct control	Primary side, direct control	V_{Batt}, I_{Batt}
	Secondary side, direct control	V_{Batt}, I_{Batt}
Indirect control	Primary side, indirect control	(V_P, I_P) or (V_S, I_S)
	Secondary side, indirect control	(V_P, I_P) or (V_S, I_S)

This review discusses both direct and indirect control strategies. For the indirect control strategy, rather than employing the complex approaches mentioned in the references, a more simplified method is adopted. This method involves deriving equations that establish the relationship between battery current and voltage with the primary and secondary tank currents and voltages, enabling effective control of the battery voltage and current.

The authors acknowledge that dual-side control is also widely used, especially in bidirectional power transfer applications[23–25]. However bidirectional control is not the focus of the current paper and will be covered separately in a different study.

Direct control

In direct control, the battery is charged by directly sensing the battery voltage and current, utilizing them as feedback signals for the controller. Depending on whether PWM is controlling the primary-side converter or the secondary-side converter, direct control can be classified into two categories: Primary-side direct control and secondary-side direct control. Both types are elaborated on in the subsequent subsection.

Primary side direct control

This is a very straightforward and easy-to-implement control technique. Figure 7 shows the block diagram of the primary side direct control of the SS-RIPT charger. V_{Batt} and I_{Batt} are used as the feedback signal for the CC-CV controller shown in Fig. 4. PWM signals generated from the CC-CV controller are used to adjust the primary side inverter output to control the voltage and current applied to the battery[15,26,27–29]. The secondary side converter could be a simple uncontrolled rectifier or should be switched to 50% duty cycle in the case of an active rectifier.

By utilizing Eqns (6) and (7), V_{Batt} and I_{Batt} can be manipulated by controlling I_P and V_P, respectively. To achieve this, a voltage control loop will generate PWM to regulate the output voltage of the inverter, ensuring that I_P remains constant, thus operating the charger in CV mode. Similarly, for CC mode, a current control loop will generate PWM to maintain a constant V_P, thereby supplying the battery with a constant I_{Batt}.

Secondary side direct control

Figure 8 shows the block diagram of the secondary side direct control scheme of the SS-RIPT system.

In Fig. 8, the primary side converter operates at a fixed 50% duty cycle to achieve a square waveform. The secondary side converter functions as an active rectifier[30–34]. For this control method to operate effectively, the secondary resonant tank must be slightly inductive[12]. PWM regulates the I_{Batt} and V_{Batt} through Eqns (2) and (3).

Indirect control

In indirect control, battery voltage and current are not used as feedback signals. Instead, primary, or secondary side resonant network variables are used as feedback signals of the CC-CV controller. Depending on whether PWM is controlling the primary-side converter or the secondary-side converter, direct control can be classified into two categories: Primary-side indirect control and secondary-side indirect control. Both types are elaborated on in the subsequent subsection.

Primary side indirect control

Figure 9 shows the block diagram of the primary side indirect control scheme of the SS-RIPT system.

In Fig. 9, the average, RMS, or peak value of V_P and I_P are detected and used as feedback signals for the CC-CV controller. Figure 10 shows the block diagram representation of the average voltage control of the CC-CV controller[35,36]. Similarly, a current controller can be implemented. Equations (6) and (7) are applicable in this control.

Secondary side indirect control

Figure 11 shows the block diagram of the secondary side indirect control scheme of the SS-RIPT system.

In Fig. 11, the primary side converter is operated at 50% duty cycle to obtain square wave output. The secondary side converter is operated as an active rectifier. Here the average, RMS, or peak values

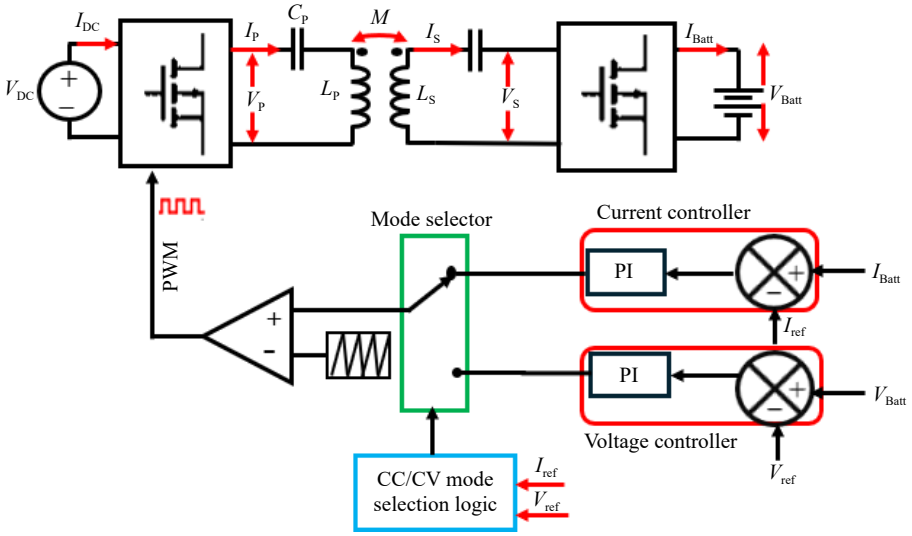

Fig. 7 Primary side direct contro.

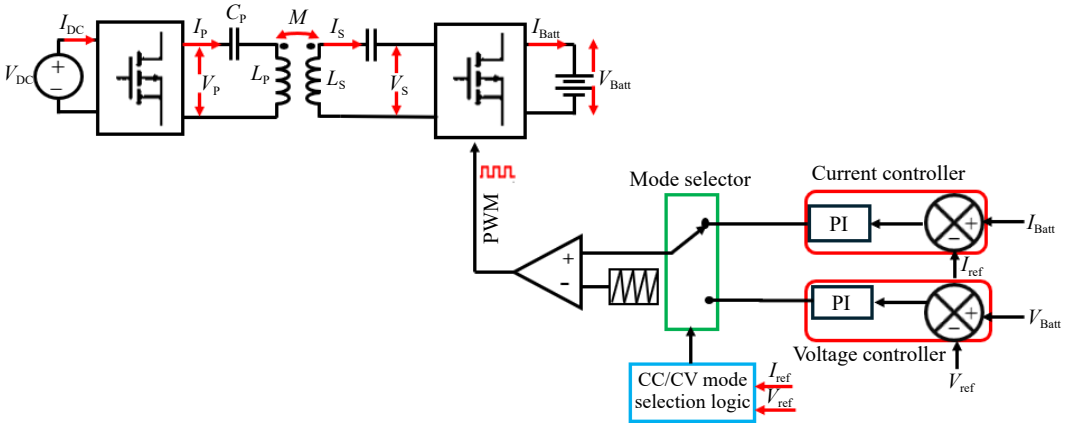

Fig. 8 Secondary side direct control.

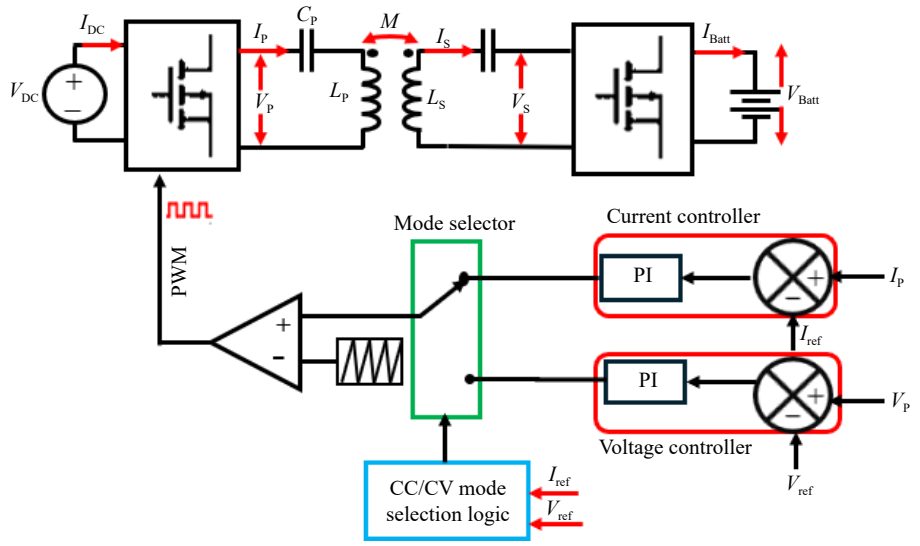

Fig. 9 Primary side indirect control.

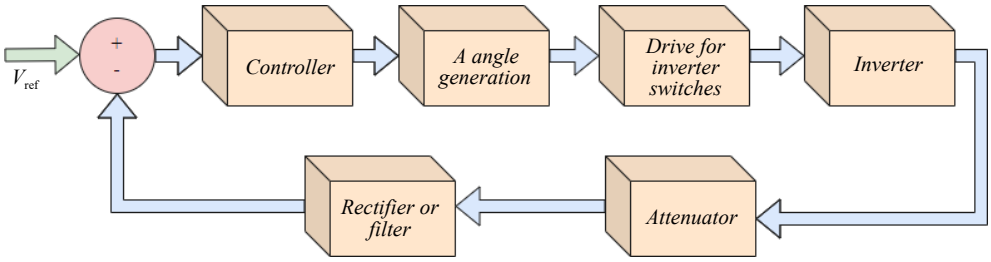

Fig. 10 Inverter output voltage regulation based on duty cycle control.

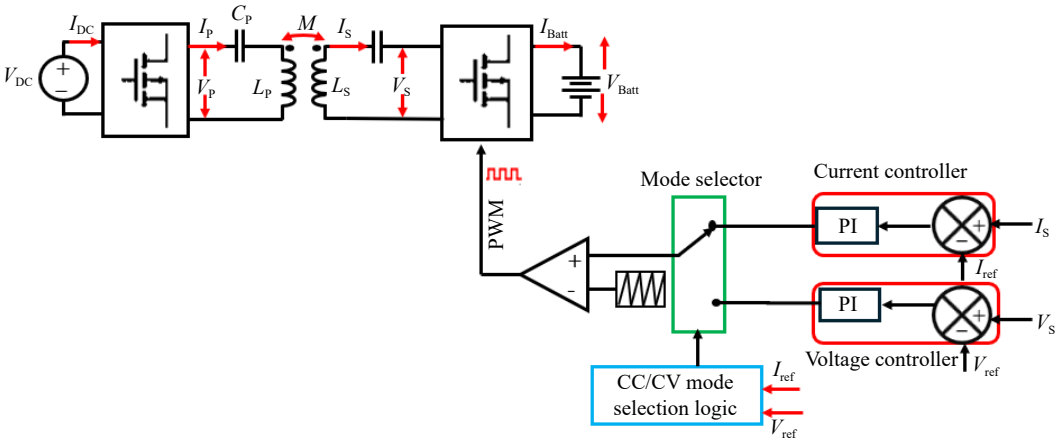

Fig. 11 Secondary side indirect control.

of V_S and I_S are detected and used as feedback signals for the CC-CV controller.

Comparison between the existing topologies

Existing literature indicates that both direct and indirect control strategies have distinct advantages and limitations. This section provides a comparison of these methods, focusing on their respective advantages and limitations.

Implementation example

Implementing all four control strategies is technically possible; however, thoroughly addressing them in a single paper is not feasible. Therefore, this paper will concentrate on showcasing the simulation and Hardware in Loop Validation of two specific strategies: primary side indirect control for CC-CV charging of Li-Ion batteries and primary side direct control for CC-CV charging of Li-Ion batteries. The simulation involves an SS-RIPT based charger simulated in PLECS, with parameters outlined in Tables 3 & 4. A comprehensive simulation circuit for the primary side indirect control is illustrated in Fig. 12.

In Table 2, the CC-CV charging profile has been decided based on 5,200 mAh 5S 25C/50C (18.5 V) Lithium Polymer battery pack[37,38].

In Fig. 12, the RMS value of I_P is sensed and used as feedback in the CV controller. For the CC controller, the RMS value of V_P is sensed and used as feedback. As stated earlier, the average, RMS, or peak value could be used.

Table 2. Comparison between direct and indirect control.

Control strategy	Advantages	Limitations
Primary side direct control	It is a straightforward and easy-to-implement control method. The direct use of battery current and voltage as feedback signals for the CC-CV controller simplifies the process of sensing DC variables. This approach reduces the weight and complexity on the receiver side.	• The dependence on wireless communication modules for information transmission incurs additional expenses associated with both hardware and software requirements • The transmitted information is vulnerable to errors, delays, and potential loss. • Strong magnetic field interference may cause instability in the communication process.
Primary side indirect control	• It eliminates the need for a dedicated communication module, thereby eliminating the risk of information loss. • The absence of a wireless communication module reduces the overall system cost.	• Sensing primary side current and voltage at high frequencies, such as 100 kHz, is difficult due to the lack of readily available sensors with sufficient bandwidth. • Indirect control strategies estimate battery current and voltage through mathematical equations rather than direct measurement, which may lead to slight discrepancies between the estimated and actual values.
Secondary side direct control	• It provides precise and robust performance without the need for communication between the receiver and transmitter. • This approach facilitates the development of control systems aimed at enhancing efficiency and optimizing power charging.	• This control approach results in increased weight and complexity on the receiver side.
Secondary side indirect control	• It does not require a dedicated communication module, thereby reducing the risk of information loss.	• Sensing secondary side current and voltage at high frequencies, such as 100 kHz, is difficult due to the lack of readily available sensors with sufficient bandwidth. • Indirect control strategies estimate battery current and voltage through mathematical equations rather than direct measurement, which may lead to slight discrepancies between the estimated and actual values.

Table 3. Specification of the SS-RIPT-based charger.

Parameters	Values
Input voltage, V_{dc}	24 V
CV mode voltage, $V_{batt,max}$	$4.2 \times 5 = 21$ V
CC mode current, I_{batt}	5 A
Minimum output voltage, $V_{Batt,min}$	$0.6 \times 21 = 12.6$ V
Maximum output power, P_{out}	$21 \times 5 = 105$ W
Switching frequency, f_{sw}	85 kHz

Table 4. Parameters of the SS-RIPT link.

Parameters	Values
Primary inductance, L_P	33.30 μH
Secondary inductance, L_S	39.73 μH
Primary capacitance for 85 kHz, C_P	105.27 nF
Secondary capacitance for 85 kHz, C_S	88.23 nF
Mutual coupling	0.20

Simulation results

This section discusses the simulation of both direct and indirect primary side control methods. The results, exported from PLECS, are plotted in MATLAB for enhanced clarity. The findings are presented in two subsections: Primary side indirect control; and Primary side direct control.

Primary side indirect control

In primary side indirect control, the primary side RMS voltage and RMS current are used to control V_{Batt} and I_{Batt}. Adjusting $IBatt_{REF}$ modifies VP_{REF} for the voltage controller while adjusting $VBatt_{REF}$ modifies IP_{REF} for the current controller.

When $IBatt_{REF}$ is changed from 5 to 3 A, the corresponding VP_{REF} is adjusted, and VP_{RMS} accurately tracks this change, as shown in Fig. 13a. Similarly, Fig. 14a demonstrates that VP_{RMS} follows VP_{REF} despite step changes in the load. Figures 13b & 14b illustrate the responses of V_P and I_P during these transitions.

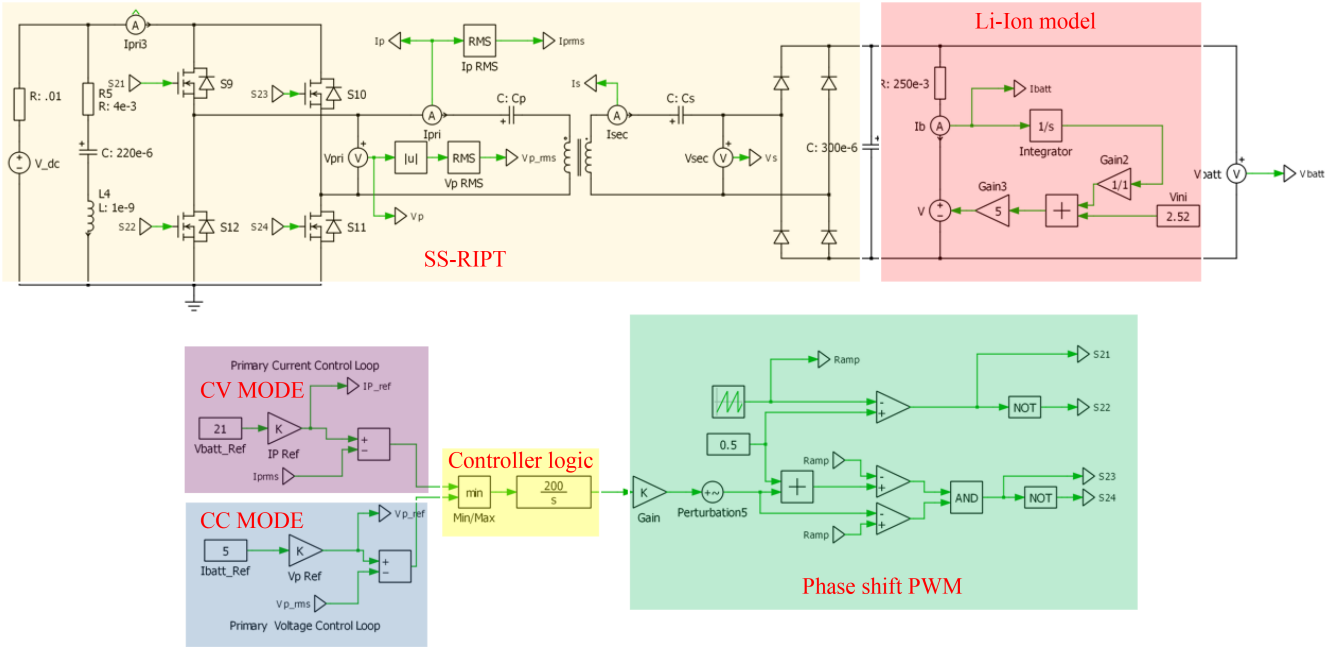

Fig. 12 PLECS simulation circuit of primary side indirect control of an Li-Ion charger using CC-CV charging.

When $VBatt_{REF}$ is changed from 21 to 12 V, the corresponding IP_{REF} is adjusted, and IP_{RMS} accurately tracks this change, as shown in Fig. 15a. Likewise, Fig. 16a demonstrates that IP_{RMS} continues to follow IP_{REF} despite step changes in the load. The responses of V_P and I_P throughout these transitions are shown in Figs 15b & 16b.

By replacing the load resistor with a Li-ion battery model designed in PLECS, as shown in Fig. 12, both controllers can operate together using logic to control the CC-CV mode of operation. The resulting performance is illustrated in Fig. 17.

Primary side direct control

In the primary side direct control approach, the V_{Batt} and I_{Batt} serve as key feedback inputs for the CC-CV controller. This controller, in turn, orchestrates the generation of the appropriate PWM signals. These signals finely tune the output of the primary side inverter, thereby precisely regulating the voltage and current delivered to the battery, ensuring optimal charging performance.

When $VBatt_{REF}$ is adjusted from 21 to 10 V and subsequently to 18 V, the corresponding V_{Batt} accurately tracks these changes, as illustrated in Fig. 18a. Similarly, Fig. 19a shows that I_{Batt} continues to follow $IBatt_{REF}$ despite step changes in the load. The responses of V_P and I_P during these transitions are depicted in Figs 18b & 19b.

Similarly, when $IBatt_{REF}$ is adjusted from 5 to 2 A and subsequently to 4A, the corresponding I_{Batt} accurately tracks these changes, as illustrated in Fig. 20a. Likewise, Fig. 21a demonstrates that I_{Batt} continues to follow $IBatt_{REF}$ despite step changes in the

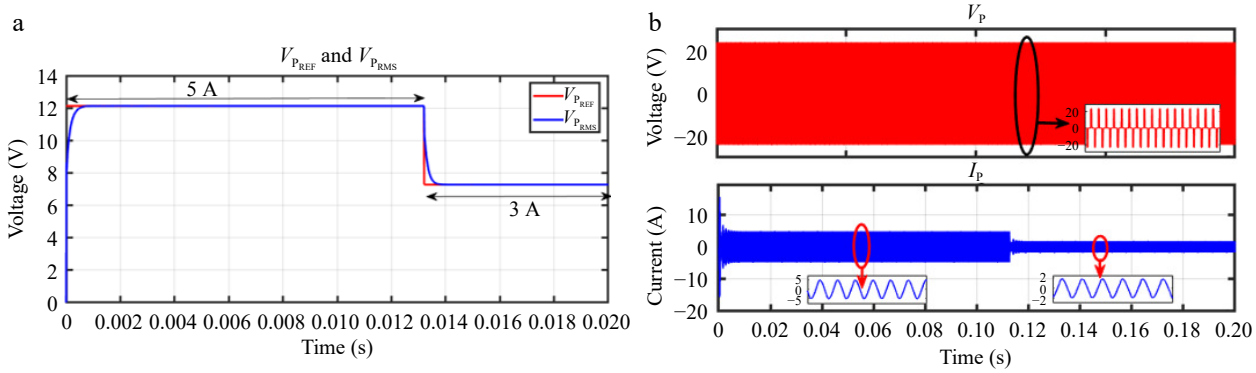

Fig. 13 Simulation result for voltage controller: (a) step change in $IBatt_{REF}$ from 5 to 3 A to change the VP_{REF}, (b) primary side voltage and current waveform for the same.

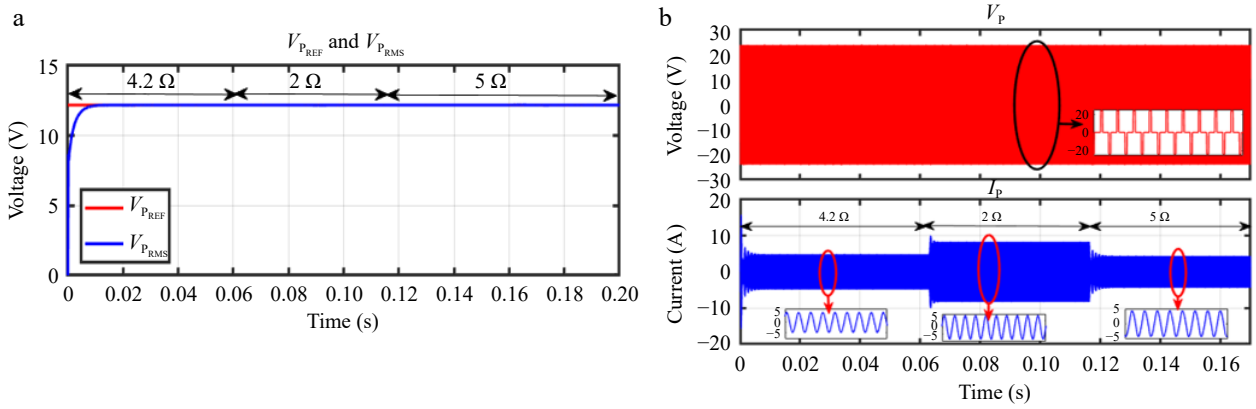

Fig. 14 Simulation result for voltage controller: (a) change in load from 4.2 to 2 to 5 Ω, (b) primary side voltage and current waveform for the same.

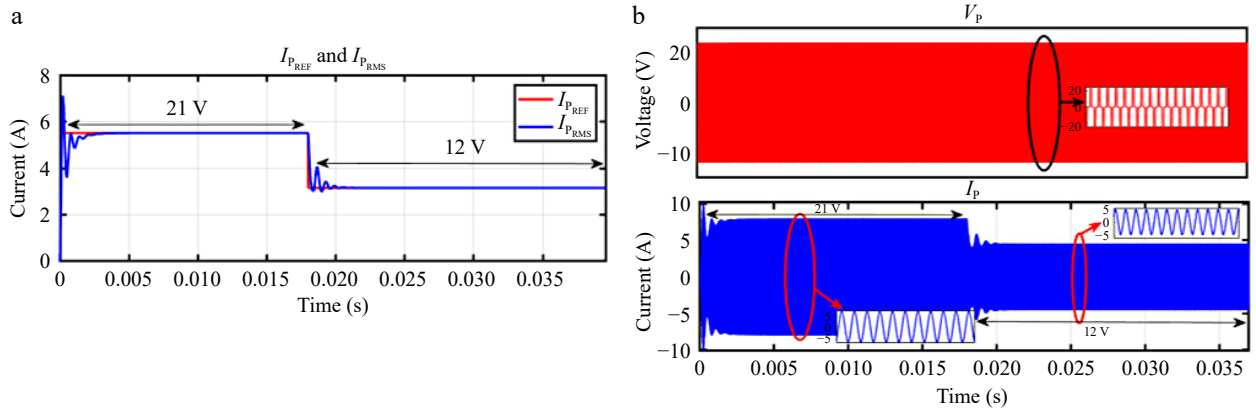

Fig. 15 Simulation result for current controller: (a) step change in $VBatt_{REF}$ from 21 to 12 V to change the IP_{REF}, (b) primary side voltage and current waveform for the same.

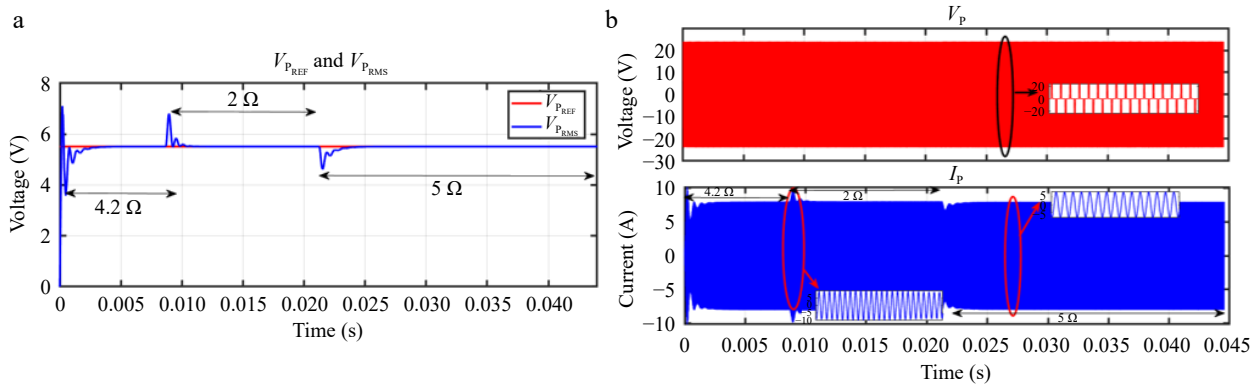

Fig. 16 Simulation result for current controller: (a) change in load from 4.2 to 2 to 5 Ω, (b) Primary side voltage and current waveform for the same.

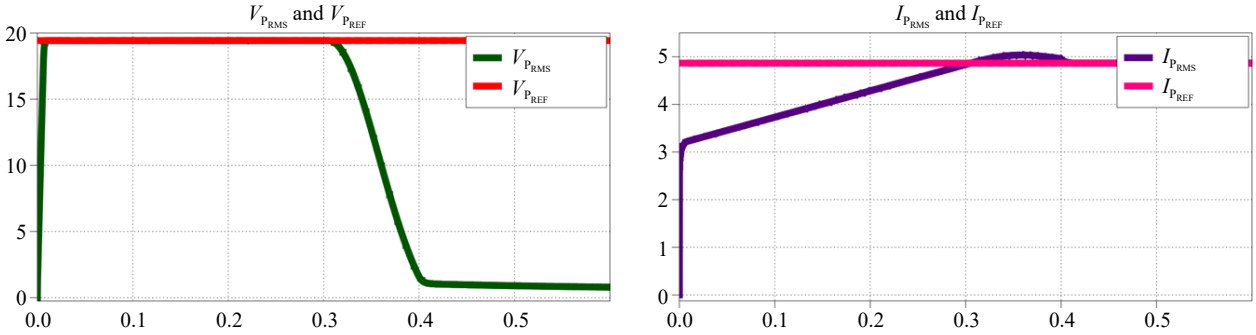

Fig. 17 CC-CV charging profile.

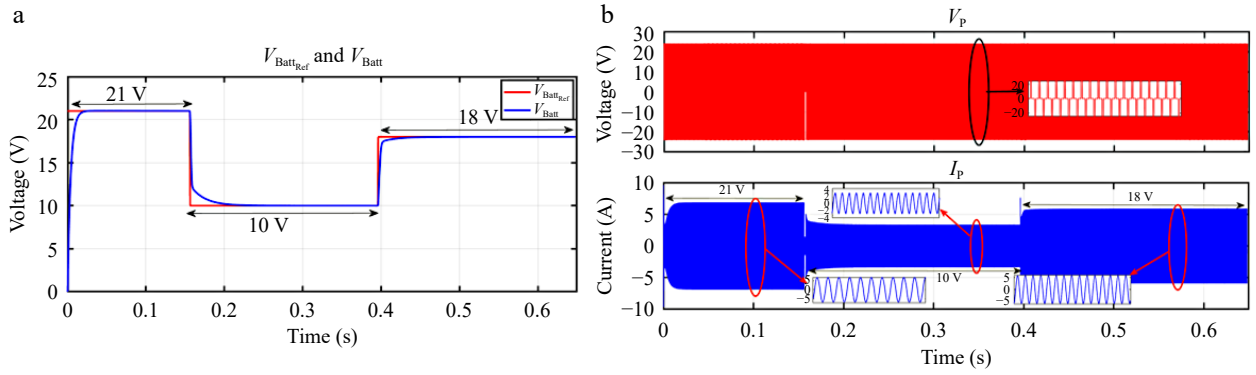

Fig. 18 Simulation result for voltage controller: (a) step change in $VBatt_{REF}$ from 21 to 10 to 18 V, (b) primary side voltage and current waveform for the same.

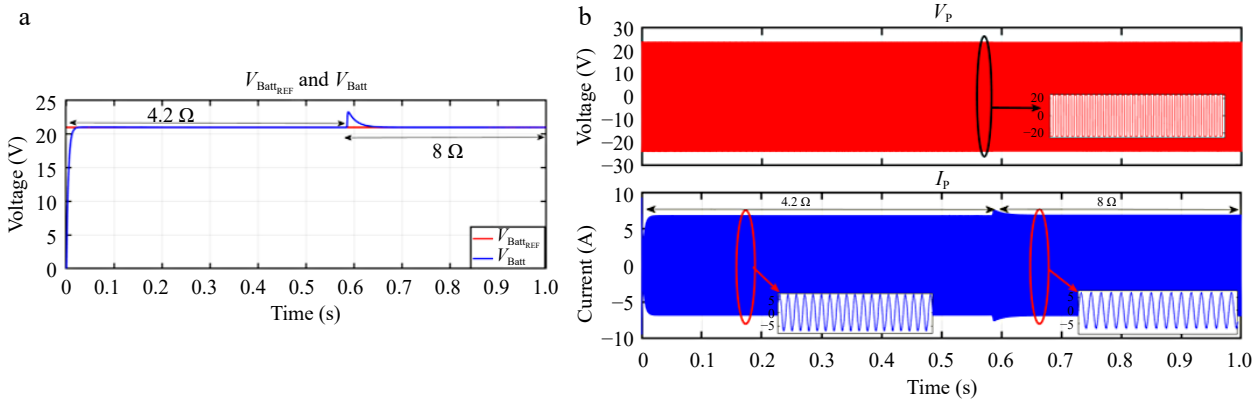

Fig. 19 Simulation result for voltage controller: (a) change in load from 4.2 to 8 Ω, (b) primary side voltage and current waveform for the same.

load. The responses of V_P and I_P during these transitions are shown in Figs 20b & 21b.

By replacing the load resistor with a Li-ion battery model designed in PLECS, as shown in Fig. 12, both controllers can operate together using logic to control the CC-CV mode of operation. The resulting performance is illustrated in Fig. 22.

Hardware-in-Loop results

The proposed control strategy is validated through Hardware-in-the-Loop (HIL) simulation using Typhoon HIL, as illustrated in Fig. 23. A digital twin of the RIPT system is developed in Typhoon HIL, with the controller implemented on a Texas Instruments TMS320F28335 DSP. The results obtained from the Typhoon HIL simulation are exported and plotted in MATLAB for enhanced clarity.

Primary side indirect control

Figures 24 & 25 display the HIL results for the voltage controller validation, demonstrating strong agreement with the simulation results depicted in Figs 13 & 14 from PLECS. Similarly, Figs 26 & 27 exhibit the HIL results for the current controller, which closely align with the PLECS simulation results shown in Figs 15 & 16.

Primary side direct control

Figures 28 & 29 present the HIL results for the voltage controller validation, showing a strong correlation with the simulation results from PLECS depicted in Figs 18 & 19. Similarly, Figs 30 & 31 display the HIL results for the current controller, which closely align with the PLECS simulation results shown in Figs 20 & 21.

A model of a Li-ion battery was created in PLECS to validate the CC-CV charging technique. The emphasis during the HIL simulation was placed on showcasing how the system adapts to changing loads, thereby underlining the effectiveness and dependability of the implemented control approach.

Conclusions

In conclusion, wireless power transfer, particularly through resonant inductive power transfer (RIPT), is gaining momentum as a convenient and efficient method for charging a variety of devices

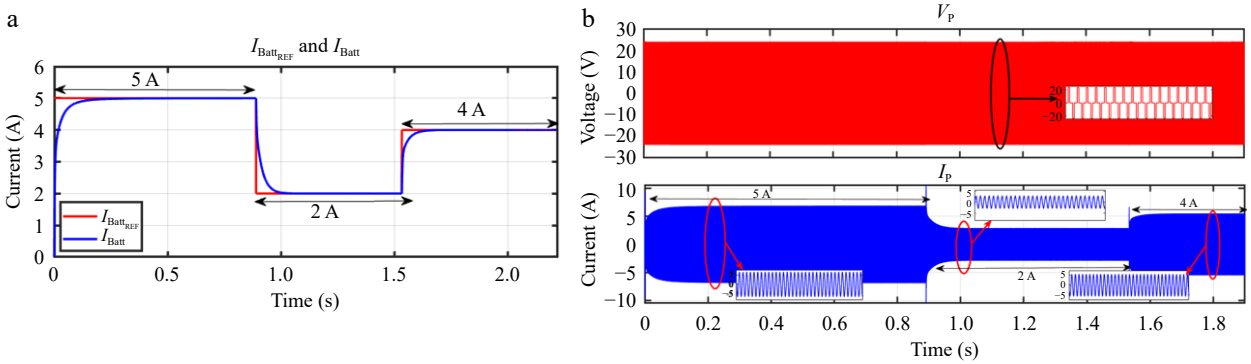

Fig. 20 Simulation result for voltage controller: (a) step change in $IBatt_{REF}$ from 5 to 2 to 4 A, (b) primary side voltage and current waveform for the same.

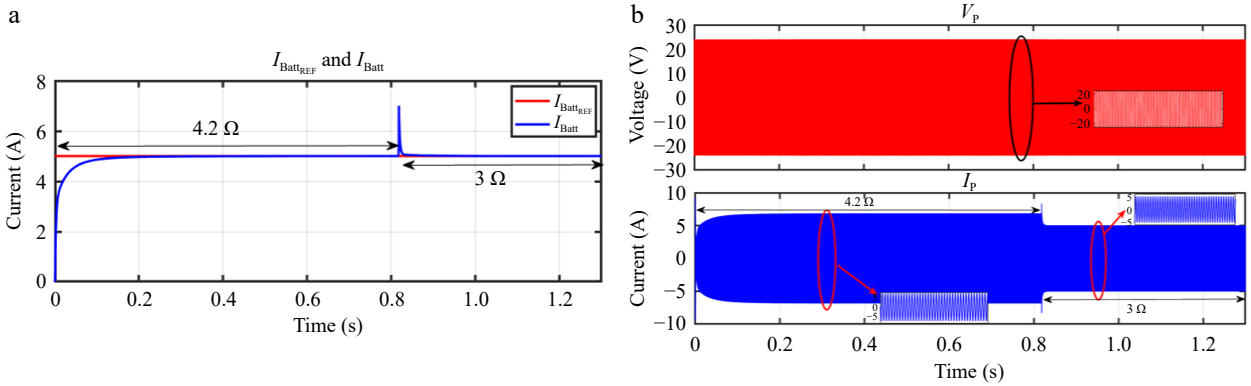

Fig. 21 Simulation result for current controller: (a) change in load from 4.2 to 3 Ω, (b) primary side voltage and current waveform for the same.

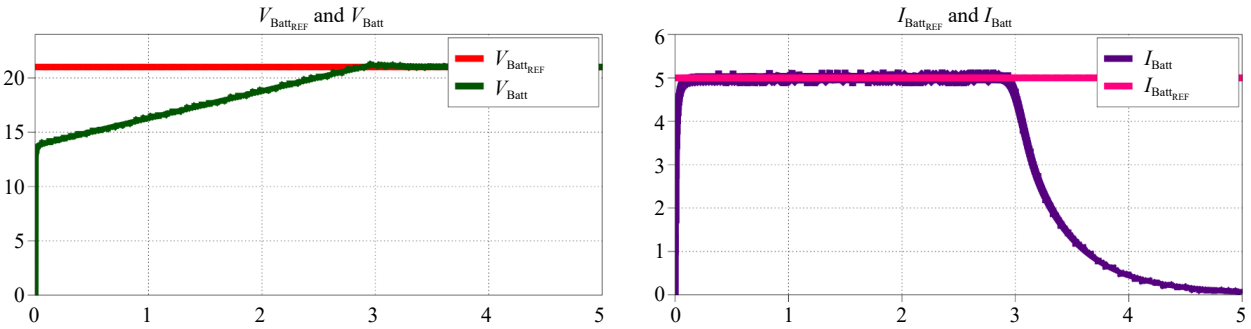

Fig. 22 CC-CV charging profile.

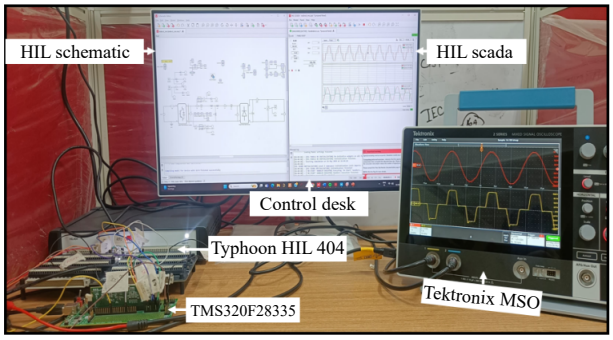

Fig. 23 Hardware in loop setup.

including Electric Vehicles (EVs), Unmanned Aerial Vehicles (UAVs), and consumer electronics such as cell phones. This technology not only provides a safe and efficient charging experience but also addresses issues such as range anxiety in EVs and extending the flight time of UAVs by eliminating the need for constant user intervention during charging. Moreover, the absence of charging cables reduces clutter and keeps charging areas organized for consumers.

The paper reviewed control methods applicable to RIPT systems for charging batteries using the Constant Current Constant Voltage (CC-CV) mode, focusing primarily on the series-series RIPT (SS-RIPT) system. It presented various control strategies, including direct and indirect control methods, and discussed their implementation for both primary and secondary sides of the RIPT system. While acknowledging the widespread use of bidirectional power transfer, the paper concentrated solely on unidirectional power transfer and left bidirectional control for future research.

This paper primarily addresses the details of primary side indirect and primary side direct control for CC-CV charging of Li-ion batteries. Both control strategies were simulated using PLECS and verified through HIL results with the DSP controller TMS320F28335 and Typhoon HIL. The feasibility and effectiveness of both controls were demonstrated through simulations and analysis, providing valuable insights for practical implementation.

Overall, this study contributes to the understanding of control strategies for RIPT systems, particularly in the context of CC-CV charging, and provides a foundation for further research and development in this field. As wireless power transfer continues to evolve, such studies are crucial for optimizing charging efficiency, improving user experience, and advancing the adoption of wireless charging technology across various applications.

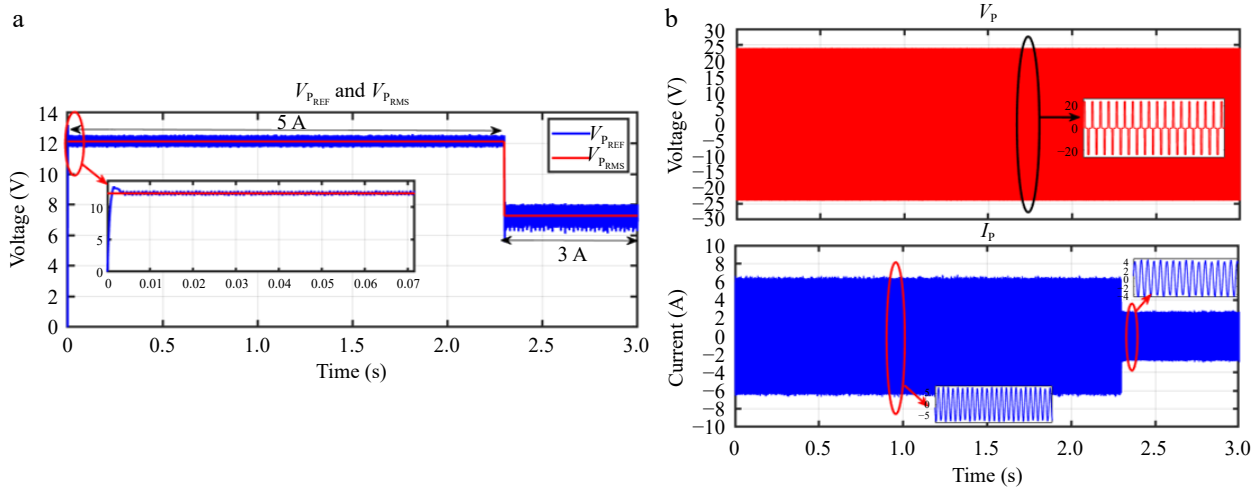

Fig. 24 HIL result for voltage controller: (a) step change in $IBatt_{REF}$ from 5 to 3 A to change the VP_{REF}, (b) primary side voltage and current waveform for the same.

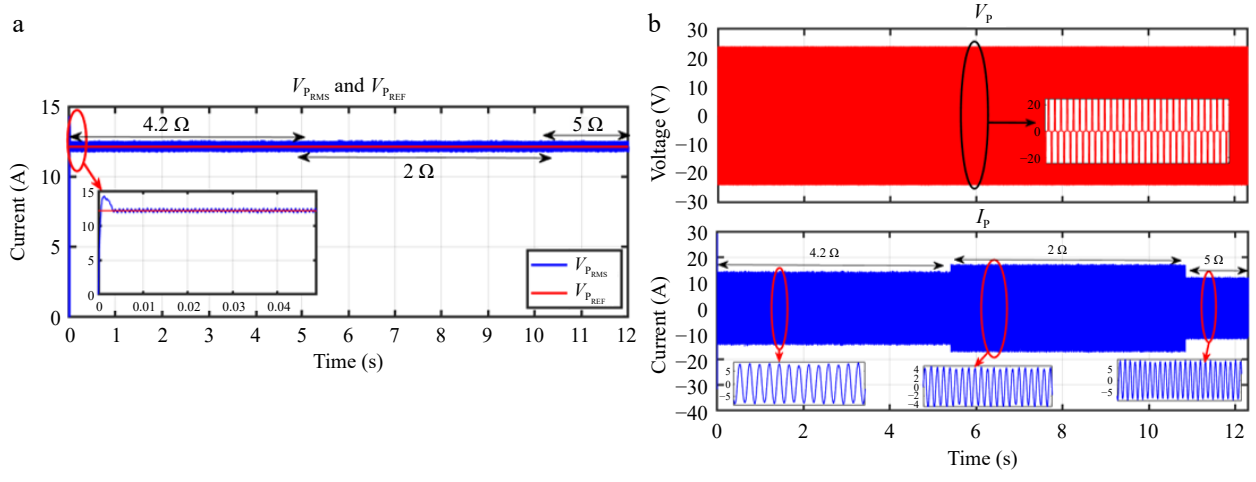

Fig. 25 HIL result for voltage controller: (a) change in load from 4.2 to 2 to 5 Ω, (b) primary side voltage and current waveform for the same.

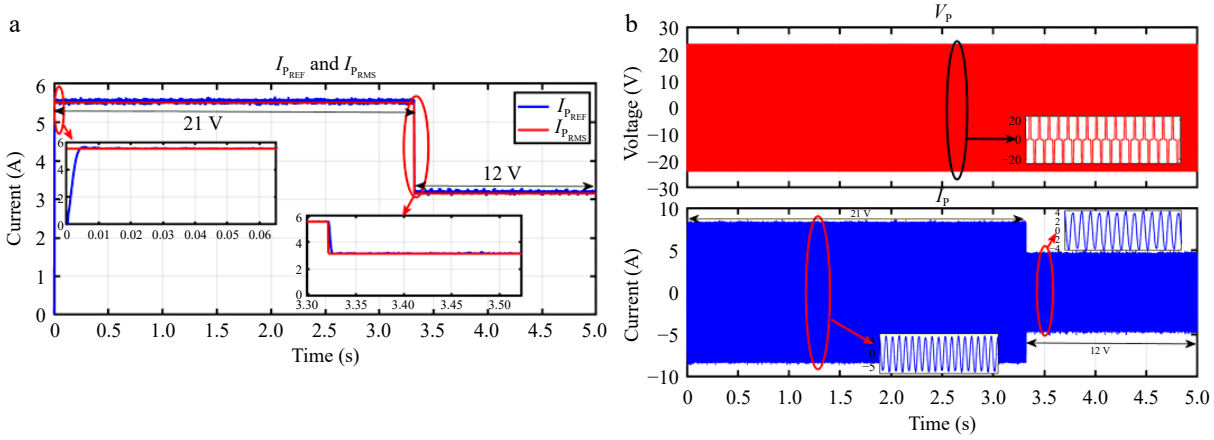

Fig. 26 HIL result for current controller: (a) step change in $VBatt_{REF}$ from 21 to 12 V to change the IP_{REF}, (b) primary side voltage and current waveform for the same.

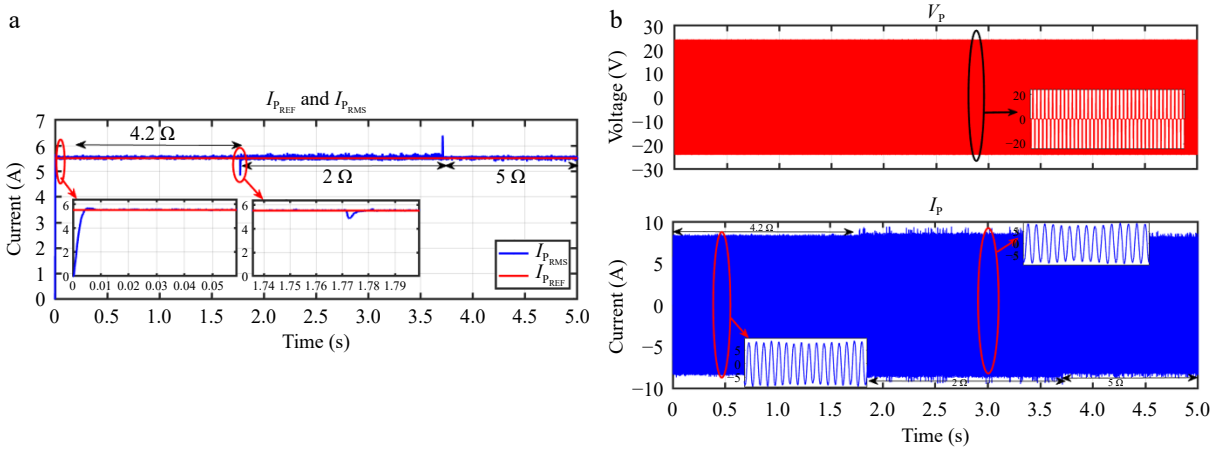

Fig. 27 HIL result for current controller: a) change in load from 4.2 to 2 to 5 Ω, (b) primary side voltage and current waveform for the same.

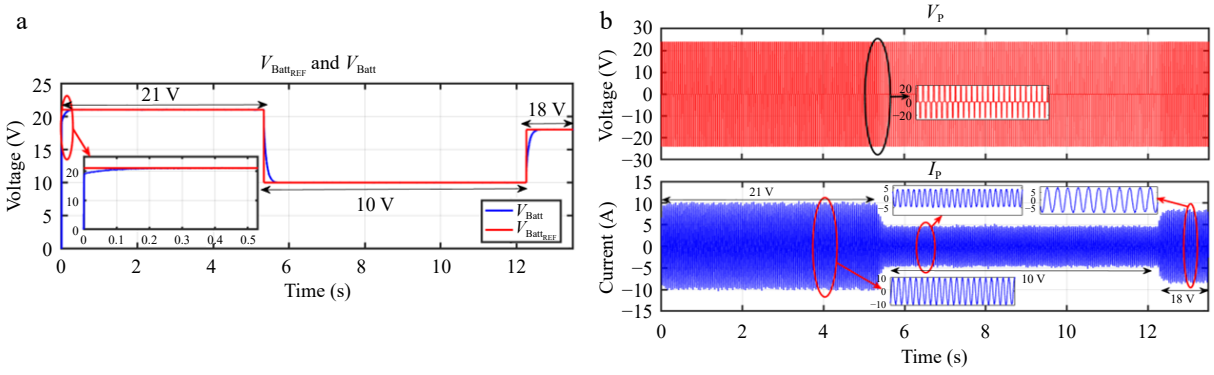

Fig. 28 HIL result for voltage controller: (a) step change in $VBatt_{REF}$ from 21 to 10 to 18 V, (b) primary side voltage and current waveform for the same.

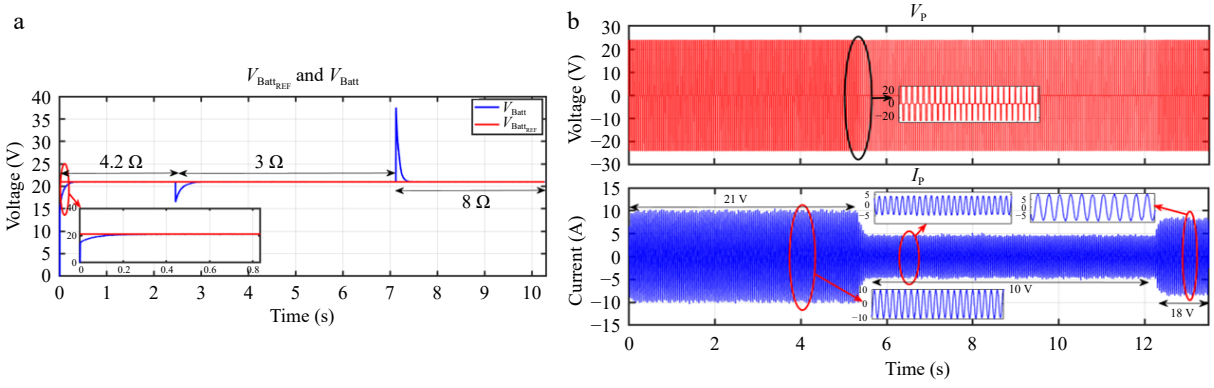

Fig. 29 HIL result for voltage controller: (a) change in load from 4.2 to 3 to 8 Ω, (b) primary side voltage and current waveform for the same.

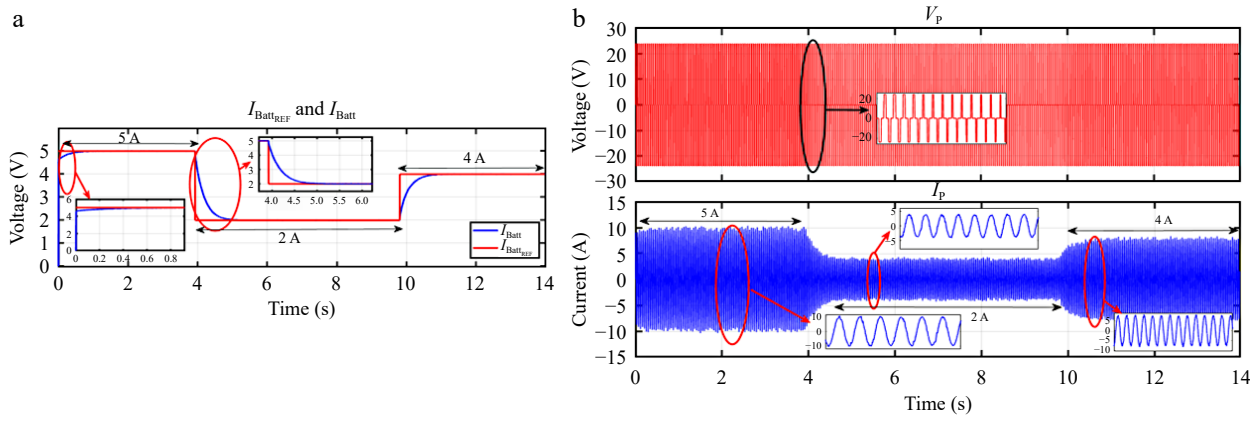

Fig. 30 HIL result for voltage controller: (a) step change in $IBatt_{REF}$ from 5 to 2 to 4 A, (b) primary side voltage and current waveform for the same.

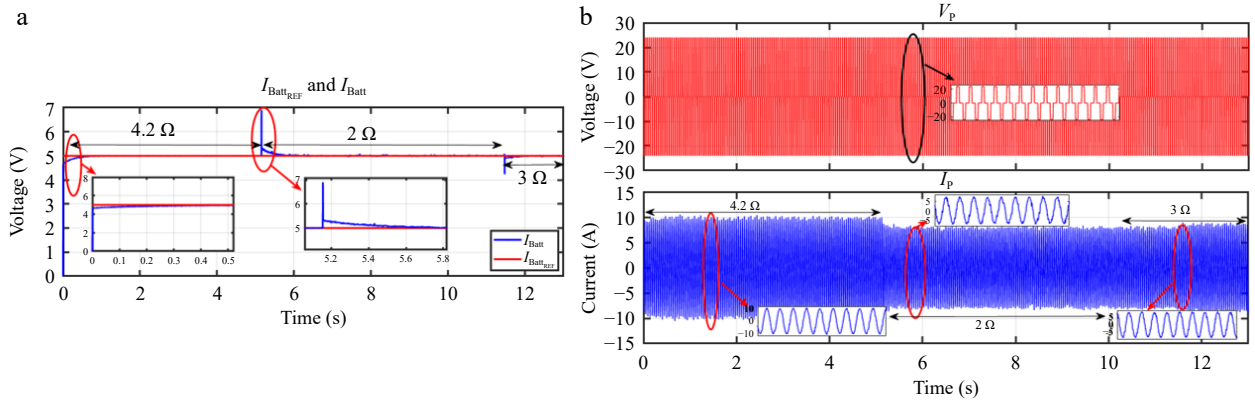

Fig. 31 HIL result for current controller: (a) change in load from 4.2 to 2 to 3 Ω, (b) primary side voltage and current waveform for the same.

Author contributions

The authors confirm contribution to the paper as follows: study conception and design: Munsi A, Pradhan S; data collection: Munsi A, Pradhan S; analysis and interpretation of results: Munsi A, Pradhan S, Aditya K; draft manuscript preparation: Munsi A, Aditya K. All authors reviewed the results and approved the final version of the manuscript.

Data availability

All data included in this study are available upon request from the corresponding author.

Acknowledgments

This research work is funded by the SEED Grant, IIT Jodhpur with grant no: I/SEED/KUA/20220126.

Conflict of interest

The authors declare that they have no conflict of interest. Kunwar Aditya is the Editorial Board member of *Wireless Power Transfer* who was blinded from reviewing or making decisions on the manuscript. The article was subject to the journal's standard procedures, with peer-review handled independently of this Editorial Board member and the research groups.

Dates

Received 29 May 2024; Revised 27 August 2024; Accepted 23 September 2024; Published online 1 November 2024

References

1. Green AW, Boys JT. 1994.10 kHz inductively coupled power transfer - concept and control. *Proceedings of 5th International Conference on Power Electronics and Variable-Speed Drives, London, UK, 26–28 October 1994*. USA: IEEE. pp. 694–99. doi: 10.1049/cp:19941049
2. Sikandar MS, Darwish M, Marouchos C. 2022. Review of wireless charging of EV. *2022 57th International Universities Power Engineering Conference (UPEC). Istanbul, Turkey, 30 August - 2 September 2022*. USA: IEEE. pp. 1–4. doi: 10.1109/UPEC55022.2022.9917793
3. Lu M, Bagheri M, James AP, Phung T. 2018. Wireless charging techniques for UAVs: a review, reconceptualization, and extension. *IEEE Access* 6:29865–84
4. Wang P, Kim J, Mutahira H, Muhammad MS. 2024. Autonomous drone control for wireless charging using power lines. *2024 18th International Conference on Ubiquitous Information Management and Communication (IMCOM). Kuala Lumpur, Malaysia, 3–5 January 2024*. USA: IEEE. pp. 1–8. doi: 10.1109/IMCOM60618.2024.10418347
5. Hannan MA, Lipu MSH, Hussain A, Mohamed A. 2017. A review of lithium-ion battery state of charge estimation and management system in electric vehicle applications: challenges and recommendations. *Renewable and Sustainable Energy Reviews* 78:834–54
6. Huang Z, Qin T, Li XL, Ding L, Iu HHC, et al. 2024. Synthesis of inductive power transfer converters with dual immittance networks for inherent CC-to-CV charging profiles. *IEEE Transactions on Power Electronics* 39:7766–77
7. Du Y, Zhang Z, Zuo Z, Wang Y. 2024. Lithium battery charging optimization via multi-stage combined charging strategy in solar-powered vehicles. *Journal of Energy Storage* 83:110716
8. Chen GJ, Liu CL, Liu YH, Wang JJ. 2024. Implementation of constant temperature–constant voltage charging method with energy loss minimization for lithium-ion batteries. *Electronics* 13:645
9. Mahesh A, Chokkalingam B, Mihet-Popa L. 2021. Inductive wireless power transfer charging for electric vehicles – a review. *IEEE Access* 9:137667–713

10. Covic GA, Boys JT. 2013. Inductive power transfer. *Proceedings of the IEEE* 101(6):1276–89
11. Liu J, Chan KW, Chung CY, Chan NHL, Liu M, et al. 2018. Single-stage wireless-power-transfer resonant converter with boost bridgeless power-factor-correction rectifier. *IEEE Transactions on Industrial Electronics* 65:2145–55
12. Rodriguez JR, Dixon JW, Espinoza JR, Pontt J, Lezana P. 2005. PWM regenerative rectifiers: state of the art. *IEEE Transactions on Industrial Electronics* 52:5–22
13. Peschiera B, Aditya K, Williamson SS. 2014. Asymmetrical voltage-cancellation control for a series-series fixed-frequency inductive power transfer system. *IECON 2014 - 40th Annual Conference of the IEEE Industrial Electronics Society. Dallas, TX, USA, 29 October - 1 November 2014*. USA: IEEE. pp. 2971–77. doi: 10.1109/IECON.2014.7048932
14. Kavimandan UD, Mahajan SM, Van Neste CW. 2021. Analysis and demonstration of a dynamic ZVS angle control using a tuning capacitor in a wireless power transfer system. *IEEE Journal of Emerging and Selected Topics in Power Electronics* 9:1876–90
15. Miller JM, Onar OC, Chinthavali M. 2015. Primary-side power flow control of wireless power transfer for electric vehicle charging. *IEEE Journal of Emerging and Selected Topics in Power Electronics* 3:147–62
16. Gati E, Kampitsis G, Manias S. 2017. Variable frequency controller for inductive power transfer in dynamic conditions. *IEEE Transactions on Power Electronics* 32:1684–96
17. Diekhans T, De Doncker RW. 2015. A dual-side controlled inductive power transfer system optimized for large coupling factor variations and partial load. *IEEE Transactions on Power Electronics* 30:6320–28
18. Madawala UK, Neath M, Thrimawithana DJ. 2013. A power–frequency controller for bidirectional inductive power transfer systems. *IEEE Transactions on Industrial Electronics* 60:310–17
19. Chow JPW, Chung HSH, Cheng CS. 2016. Use of transmitter-side electrical information to estimate mutual inductance and regulate receiver-side power in wireless inductive link. *IEEE Transactions on Power Electronics* 31:6079–91
20. Madawala UK, Thrimawithana DJ. 2012. New technique for inductive power transfer using a single controller. *IET Power Electronics* 5:248
21. Song K, Li Z, Jiang J, Zhu C. 2018. Constant current/voltage charging operation for series–series and series–parallel compensated wireless power transfer systems employing primary-side controller. *IEEE Transactions on Power Electronics* 33:8065–80
22. Li Z, Liu H, Tian Y, Liu Y. 2021. Constant current/voltage charging for primary-side controlled wireless charging system without using dual-side communication. *IEEE Transactions on Power Electronics* 36:13562–77
23. Zhang Y, Chen S, Li X, Tang Y. 2021. Dual-side phase-shift control of wireless power transfer implemented on primary side based on driving windings. *IEEE Transactions on Industrial Electronics* 68(9):8999–9002
24. Jia S, Chen C, Duan S, Chao Z. 2021. Dual-side asymmetrical voltage-cancelation control for bidirectional inductive power transfer systems. *IEEE Transactions on Industrial Electronics* 68(9):8061–71
25. Wu M, Yang X, Chen W, Wang L, Jiang Y, et al. 2021. A dual-sided control strategy based on mode switching for efficiency optimization in wireless power transfer system. *IEEE Transactions on Power Electronics* 36(8):8835–48
26. Thrimawithana DJ, Madawala UK. 2010. A primary side controller for inductive power transfer systems. *2010 IEEE International Conference on Industrial Technology. Via del Mar, Chile, 14–17 March 2010*. USA: IEEE. pp. 661–66. doi: 10.1109/ICIT.2010.5472724
27. Wang C, Zhu C, Song K, Wei G, Dong S, et al. 2017. Primary-side control method in two-transmitter inductive wireless power transfer systems for dynamic wireless charging applications. *2017 IEEE PELS Workshop on Emerging Technologies: Wireless Power Transfer (WoW). Chongqing, China, 20–22 May 2017*. USA: IEEE. pp. 1–6. doi: 10.1109/WoW.2017.7959366
28. Liu Y, Madawala UK, Mai R, He Z. 2021. Primary-side parameter estimation method for bidirectional inductive power transfer systems. *IEEE Transactions on Power Electronics* 36:68–72
29. Aditya K, Williamson SS. 2015. Advanced controller design for a series-series compensated inductive power transfer charging infrastructure using asymmetrical clamped mode control. *2015 IEEE Applied Power Electronics Conference and Exposition (APEC). Charlotte, NC, USA, 15–19 March 2015*. USA: IEEE. pp. 2718–24. doi: 10.1109/APEC.2015.7104735
30. Lovison G, Imura T, Hori Y. 2016. Secondary-side-only simultaneous power and efficiency control by online mutual inductance estimation for dynamic wireless power transfer. *IECON 2016 - 42nd Annual Conference of the IEEE Industrial Electronics Society. Florence, Italy, 23–26 October 2016*. USA: IEEE. pp. 4553–58. doi: 10.1109/IECON.2016.7793790
31. Pang B, Deng J, Liu P, Wang Z. 2017. Secondary-side power control method for double-side LCC compensation topology in wireless EV charger application. *IECON 2017 - 43rd Annual Conference of the IEEE Industrial Electronics Society. Beijing, China, 29 October - 1 November 2017*. USA: IEEE. pp. 7860–65. doi: 10.1109/IECON.2017.8217377
32. Hatchavanich N, Sangswang A, Konghirun M. 2020. Secondary-side voltage control via primary-side controller for wireless EV chargers. *IEEE Access* 8:203543–54
33. Madawala UK, Neath M, Thrimawithana DJ. 2013. A power–frequency controller for bidirectional inductive power transfer systems. *IEEE Transactions on Industrial Electronics* 60(1):310–17
34. Tang Y, Chen Y, Madawala UK, Thrimawithana DJ, Ma H. 2018. A new controller for bidirectional wireless power transfer systems. *IEEE Transactions on Power Electronics* 33(10):9076–87
35. Cai J, Sun P, Ji K, Wu X, Ji H, et al. 2024. Constant-voltage and constant-current controls of the inductive power transfer system for electric vehicles based on full-bridge synchronous rectification. *Electronics* 13(9):1686
36. Shipra K, Maurya R. 2024. Brayton-Moser passivity-based controller for an on-board integrated electric vehicle battery charger. *Journal of Energy Storage* 75:109652
37. Aditya K. 2023. Sizing wireless battery charger for the CC-CV charging of lithium polymer battery used in unmanned aerial vehicle. *2023 IEEE 3rd International Conference on Sustainable Energy and Future Electric Transportation (SEFET). Bhubaneswar, India, 9-12 August 2023*. USA: IEEE. pp. 1–6. doi: 10.1109/SeFeT57834.2023.10245551
38. Pradhan S, Munsi A, Aditya K. 2023. Ensuring safe and reliable wireless charging of unmanned aerial vehicles: the imperative for foreign object detection methods. *2023 IEEE 3rd International Conference on Sustainable Energy and Future Electric Transportation (SEFET). Bhubaneswar, India, 9–12 August 2023*. USA: IEEE. pp. 1–6. doi: 10.1109/SeFeT57834.2023.10245524